The Evaluation of a New Method to Detect Mixing Layer Heights Using Lidar Observations

MICHEAL HICKS

National Weather Service, Sterling, Virginia

RICARDO SAKAI AND EVERETTE JOSEPH

Howard University, Washington, D.C.

(Manuscript received 8 May 2014, in final form 8 May 2015)

ABSTRACT

A new automatic mixing layer height detection method for lidar observations of aerosol backscatter profiles is presented and evaluated for robustness. The new detection method incorporates the strengths of Steyn et al.'s error function–ideal profile (ERF) method and Davis et al.'s wavelet covariance transform (WCT) method. These two methods are critical components of the new method, and their robustness is also evaluated and then contrasted to the new method. The new method is applied to aerosol backscatter observations in two ways: 1) by looking for the most realistic mixing height throughout the entire profile and 2) by searching for mixing height below significant elevated obscurations (e.g., clouds or aerosol layers). The first approach is referred to as the hybrid method and the second as the hybrid-lowest method. Coincident radiosounding observations of mixing heights are used to independently reference the lidar-based estimates.

There were 4030 cases examined over a 5-yr period for mixing heights. The efficacy of the lidar-based methods was determined based on diurnal, seasonal, stability, and sky obscuration conditions. Of these conditions, the hybrid method performed best for unstable and cloudy situations. It determined mixing heights reliably (less than ±0.30-km bias) for close to 70% of those cases. The hybrid-lowest method performed best in stable and clear-sky conditions; it determined mixing heights reliably for over 70% of those cases. The WCT method performed the best overall.

1. Introduction

The mixing layer (ML) is responsible for the exchanges of heat, moisture, momentum, aerosols, and greenhouse gases from the surface to adjacent atmospheric layers and vice versa (Seibert et al. 2000). The budget of these exchanges is critical to dispersion, weather, and climate forecasting (Seibert et al. 2000; Liu and Liang 2010). In atmospheric forecast models, the ML height is commonly used to scale the intensity of boundary layer turbulence, which can consequently impact the budget of these exchanges (Seibert et al. 2000; Liu and Liang 2010). This study defines ML height as the height of the lowest layer of the atmosphere, adjacent to the surface, that can mix pollutants or any atmospheric constituents emitted or entrained into it by mechanical and/or convection turbulence in a relatively short period of time, roughly 1–2 h (Baxter 1991; Beyrich 1997; Seibert et al. 2000; Luo et al. 2014). This definition is used to evaluate automatic ML height detection methods designed for lidar observations.

Lidars can continuously monitor the distributions of atmospheric tracers for the detection of ML heights (Emeis et al. 2008). Automatic detection methods are commonly used to attain these heights in a timely manner (e.g., Schmid and Niyogi 2012; Granados-Muñoz et al. 2012; Luo et al. 2014). In general, there are no standard practices for determining ML heights (Seibert et al. 2000) and the approach taken depends on what is being measured (e.g., thermodynamic variables or aerosol content; Seidel et al. 2010). Lidars often measure aerosol content to attain ML heights. Hence, lidar-based detection methods (H_L) normally exploit the disparity of aerosol loading in the ML relative to the adjacent atmosphere to locate ML height. Some of the

Corresponding author address: Micheal Hicks, National Weather Service, 43741 Weather Service Rd., Sterling, VA, 20166. E-mail: micheal.m.hicks@noaa.gov; ricardo.k.sakai@howard.edu; ejosgm@gmail.com

DOI: 10.1175/JTECH-D-14-00103.1

most popular H_L methods include the gradient (Senff et al. 1996; Flamant et al. 1997; Menut et al. 1999), temporal variance (Piironen and Eloranta 1995), backscatter threshold (Melfi et al. 1985; Boers et al. 1984), error function-ideal profile (ERF; Steyn et al. 1999), and wavelet covariance transform (WCT; Davis et al. 1997, 2000) methods. In general, these methods can reliably identify significant gradient layers (aerosol, cloud, etc.) within a backscatter profile but does not always attribute the most appropriate layer to ML height (due to residual layers, signal noise, etc.). Hageli et al. (2000) suggest using H_L methods jointly to improve their layer attribution efficiency (e.g., Hennemuth and Lammert 2006; Martucci et al. 2007; Angelini et al. 2009). Hence, a new detection method based on that concept is presented.

The new method is composed of the WCT and ERF methods. The robustness of the new method is evaluated over a long-term dataset for various meteorological conditions and contrasted to the robustness of the WCT and ERF methods. Coincident radiosonde-based observations of ML height (H_{RS}) are used to compare to the H_L methods and serve as an independent reference. The efficacy of the new method is characterized in this study and its preferred meteorological conditions are identified.

In the subsequent sections the following is presented: Section 2, the test site and instrumentation used; section 3, the new H_L method and H_{RS} method; section 4, the results; and section 5, a summary and discussion of findings.

2. Site characteristics and instrumentation

Lidar measurements are obtained from the Atmospheric Radiation Measurement Program (ARM) at the Southern Great Plains (SGP) Central Facility (Stokes and Schwartz 1994) in Lamont, Oklahoma (36°36′18.0″N, 97°29′6.0″W). This rural site has a flat grassland terrain at 0.32 km above sea level. At this site, ARM has maintained a comprehensive suite of atmospheric measurements of high data quality. Its autonomous Raman lidar (RL) and radiosounding measurements from 2006 to 2010 are of primary interest. The RL operated for over 90% of the time during this evaluation period (2006–10). The radiosounding observations were also consistently available, with a release point approximately 0.10 km away from the RL.

The autonomous RL system uses a powerful triple Nd:YAG laser (12-W output) that transmits at the third harmonic wavelength (355 nm). It has a dual field of view (FOV) and can retrieve backscatter from atmospheric constituents above 0.80 km with a complete receiver overlap (Goldsmith et al. 1998). The backscattered information retrieved is used to derive several data products (Ferrare et al. 2006). Automatic value-added procedures (VAPs) are used to correct these data products for issues such as the system's incomplete overlap and solar daytime noise; in addition to merging the backscatter observations from the system's dual-FOV detectors [see Turner et al. (2002) for more VAP details].

The autonomous RL data product of aerosol scattering ratio (ASR) is used to detect ML heights and evaluate the H_L methods. ASR is defined as the ratio of the sum of total molecular and aerosol backscatter return to molecular return $[\beta_m(\lambda, z) + \beta_a(\lambda, z)]/\beta_m(\lambda, z)$. Its dependence on aerosols resembles that of data products from weaker (less signal to noise) but more prevalent elastic lidar systems [i.e., Vaisala ceilometer (1-mW output), micropulse lidar (25-mW output), etc.], and therefore results attained should also be applicable to them. The overlap correction applied to ASR measurements has a 5% uncertainty and can effectively maintain the vertical distribution of the actual aerosol content (e.g., Turner et al. 2002; Revercomb et al. 2003). The temporal and spatial resolution of the ASR data product is 10 min and 0.075 km below 3 km and 0.15 km above 3 km, respectively (ARM 1994, 2004).

The radiosoundings are conducted 4 times daily, roughly every 6 h (http://www.arm.gov/instruments/sonde). These soundings provide atmospheric in situ data with a temporal resolution of 2 s and an ascent rate of 5 m s^{-1}. The radiosonde used is the Vaisala model RS92-SGP and it is tracked by the Vaisala DigiCORA III ground station.

3. Determination and comparison of mixing layer heights

The ability of the new WCT and ERF H_L methods to determine ML height is evaluated by comparing them to independent observations from coincident H_{RS} measurements. The comparison results are categorized by meteorological conditions to identify the most optimal conditions for the H_L methods. The following subsections describe the new H_L method, the H_{RS} method, and the methodology used to compare H_L and H_{RS} along with error considerations.

a. Lidar detection method

The WCT and ERF methods were selected as components of the new method because of their applicability to single-backscatter profiles (Menut et al. 1999) and complementary relationship, with the WCT method being more sensitive to small-scale structures and fluctuations in

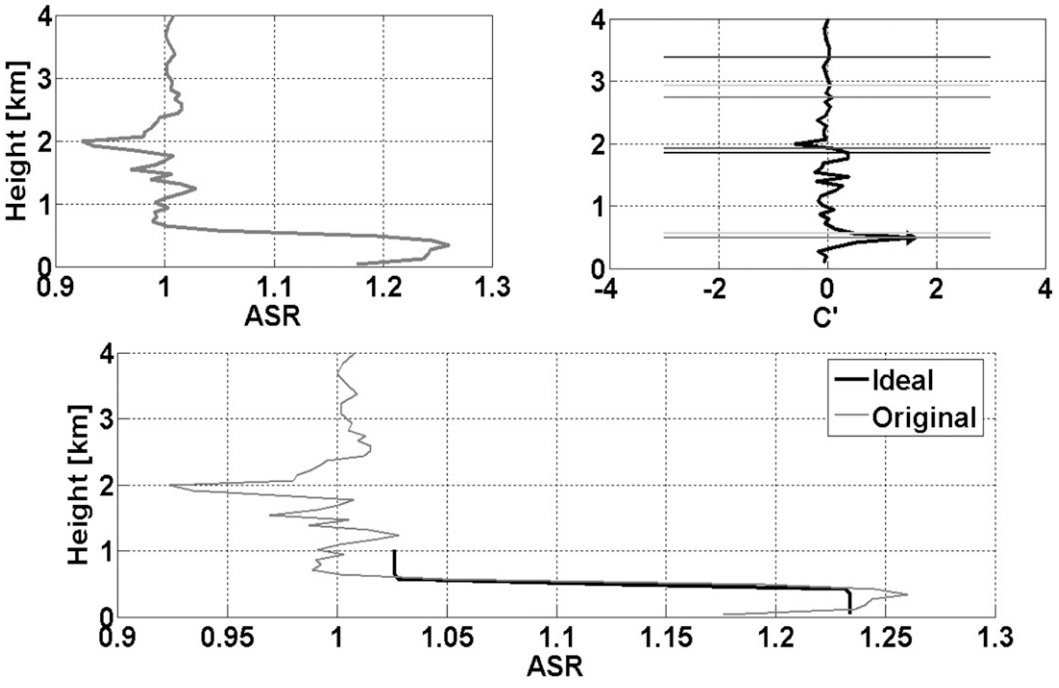

FIG. 1. An example of the hybrid method process during an unstable afternoon. (a) A typical ASR profile. (b) The covariance transform of the ASR profile. The solid horizontal lines overlaid on top of the covariance transform are local maximums of the transform profile. They represent potential mixing heights that are ingested into a modified ERF algorithm. (c) The overlaid best-fit ideal profile.

backscatter profiles (Emeis et al. 2008). They are combined such that the WCT method detects the significant gradient layers and the ERF method determines which of the layers correspond to ML height. The use of these two methods (called "component methods") in this manner is referred to as the hybrid method.

The application of the hybrid method is performed in four steps, and Fig. 1 provides an example of those steps. Figure 1a displays a typical ASR profile observed over SGP. Figure 1b describes the first two steps of the method: step 1, the WCT method is applied, with a wavelet basis set dilation that is equal to the spatial resolution of the profile under evaluation, to produce a covariance transform (C') profile; and step 2, several maxima of C' are identified as first guesses of ML height (denoted as g–z') by incrementing subsequently throughout the profile in 1-km layers, starting from the surface and continuing 0.10 km above the preceding g–z'. For step 3, the 1-km g–z' layers are ingested into a modified ERF algorithm. Steyn et al. (1999) defines the ERF algorithm as

$$B(z) = \frac{(B_{\mathrm{ML}} + B_{\mathrm{FT}})}{2} - \frac{(B_{\mathrm{ML}} - B_{\mathrm{FT}})}{2}\,\mathrm{erf}\left[\frac{(z + z_m)}{s}\right], \quad (1)$$

where $B(z)$ is the ideal ML backscatter profile, B_{ML} is the average backscatter of the ML, B_{FT} is the mean backscatter of the free troposphere, erf is the error function, z is height, z_m is ML height, and s is proportional to the thickness of the transition zone. This study's modified ERF algorithm uses g–z' as z_m in 1-km layers. An example of a best-fit $B(z)$ profile, using the modified ERF algorithm, is provided in Fig. 1c. Last, of the g–z' guesses, the H_L estimate is chosen based on 1) the root-mean-square error (RMSE) of the ideal and measured backscatter profiles (Steyn et al. 1999); 2) the magnitude of C' corresponding to the respective g-z'; and 3) the difference between the bottom half ("ML") and top half ("free troposphere") of the ideal profile ($B_{\mathrm{ML–FT}}$). It is equated as

$$\xi_i = \frac{\mathrm{RMSE}_i}{(B_{\mathrm{ML–FT}_i} \times C'_i)^2}, \quad (2)$$

where ξ is the H_L determining parameter and i is the height index. The g–z' corresponding to minimum ξ is selected as H_L. For the remainder of this section, the hybrid method's H_L estimate will be denoted as HH_L.

The hybrid-lowest method is an extension of the hybrid method and is also evaluated in this analysis. This method is designed to look for a minimum C' (valley gradient) below HH_L in the backscatter profile under inspection. To identify valley gradients, not only is a wavelet basis set dilation of the profile's resolution used

TABLE 1. Empirical constants (km), added to the surface-based LCL height approximations per season and diurnal period.

	Winter (km)	Spring (km)	Summer (km)	Autumn (km)
Night	0	0	0	0
Morning	0.5	0.5	0.5	0.5
Day	0.5	1	1.5	1
Evening	0.5	0.5	1	0

for C', but also a dilation that is 3 times its spatial resolution (denoted as $3\Delta C'$). A valley gradient found beneath HH_L, determined by C' or $3\Delta C'$, is believed to indicate the base of an elevated obscuration (i.e., an aerosol or cloud layer). If a valley gradient is discovered, then the hybrid-lowest method assumes HH_L to be an overestimate and selects the height of the maximum C' (peak gradient) below the valley gradient as H_L; otherwise, it accepts HH_L as the ML height. This study also evaluates the efficacy of the component methods. The minimum RMSE component of Eq. (2), corresponding to g–z', is used to determine H_L for the modified ERF method.

Height constraints are utilized with the H_L detection methods to minimize interference from elevated obscurations (e.g., high clouds). The height constraint method used is based on a lifting condensation level (LCL) height approximation, which is approximated from surface air and dewpoint temperatures and an assumption of dry-adiabatic lapse rate (Lawrence 2005). Empirical constants are also added to these LCL height approximations to ensure they clear the height of the ML, due to the LCL height approximations sometime being calculated below ML heights, as determined by H_{RS}. The empirical constants are added according to season and diurnal period; Table 1 provides their respective values. They range from 0 km for nighttime conditions to 1.5 km for midday summer conditions. These constants were found suitable for SGP based on H_{RS} comparisons. In addition, the hybrid-lowest method uses this height constraint technique to limit the range used to locate the minimum gradient of a backscatter profile.

b. Radiosonde detection method

A radiosonde sounding of thermodynamic and dynamic atmospheric variables can be used as a turbulence proxy for determining ML height. Popular methods to do this include examining significant gradients from profiles of these measured atmospheric variables, such as virtual potential temperature (θ_v), specific humidity (q), and wind speed (M) profiles, or the use of parameterization methods, such as the bulk Richardson number (Ri_B) method. This analysis uses the Ri_B method to estimate H_{RS} (Seidel et al. 2012) and the profile gradient methods (θ_v, q, and M) to quality control H_{RS}.

The Ri_B method assumes continuous turbulence (steady state), and the height where this turbulence decreases beyond a critical value ($\mathrm{Ri}_{\mathrm{Bc}}$) is considered the height of the ML (Zilitinkevich and Baklanov 2002). Studies have found $\mathrm{Ri}_{\mathrm{Bc}}$ to be site and stability dependent due to surface roughness and topography characteristics. In the literature, $\mathrm{Ri}_{\mathrm{Bc}}$ values range from 0.03 over a relatively smooth homogenous surface to 7.2 over a rough heterogeneous surface (Jeričević and Grisogono 2006). This study takes place over a relatively smooth and homogenous surface, and the empirical $\mathrm{Ri}_{\mathrm{Bc}}$ constants of 0.01 for unstable conditions, 0.05 for near-neutral conditions, and 0.25 for stable conditions were found suitable based on comparisons to θ_v, q, and M observations. Also, before applying the Ri_B method, the radiosounding observations are block averaged into 0.03-km layers to remove nonsmooth data points. Last, H_{RS} is quality controlled by requiring it to measure within ± 0.25 km of at least one of the profile gradient methods (θ_v, q, or M). If this criterion is not met, then the corresponding case is excluded from the analysis.

c. Comparative approach

The use of H_{RS} measurements to evaluate H_L is a common practice (e.g., Hennemuth and Lammert 2006; Martucci et al. 2007; Haeffelin et al. 2012; Granados-Muñoz et al. 2012; Yang et al. 2013; Luo et al. 2014), and this study differs by conducting its evaluation over a long-term dataset that covers a large range of meteorological conditions. The H_L methods of this study were applied to ASR profiles that were temporally averaged over 20-min periods, with the release times of coincident radiosoundings being the start of the periods. An averaging period of 20 min was used to ensure ample time for radiosoundings to reach the height of H_{RS} before comparing to H_L. The primary errors to consider when comparing H_{RS} to H_L include the following: 1) differences in lateral locations, as H_{RS} and H_L are often horizontally displaced as a result of the radiosounding balloon drift; and 2) differences in sampled volumes, as the radiosounding provides an instantaneous observation and the lidar an average. The error caused by the balloon drift should be negligible, since the horizontal distance traveled on average before reaching H_{RS} is relatively small (92% drifted less than 2 km) compared to SGP's mostly homogeneous surface condition. Conversely, this comparison will be subjected to random errors due to the differences in the sampled volumes. Fortunately, each H_L method should be impacted equally by the random errors and should not bias the results.

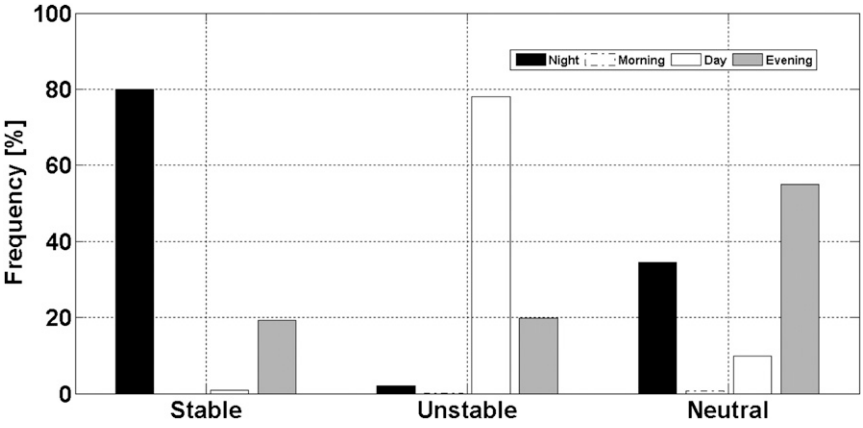

FIG. 2. The distribution of cases examined to evaluate the mixing height detection methods. The distribution is of diurnal periods by atmospheric stability conditions.

The H_L and H_{RS} intercomparison results are placed in categories according to season, diurnal period, atmospheric stability, and sky obscuration conditions. This is done to identify the preferred meteorological conditions of the H_L methods. The seasons are defined by their meteorological definition [i.e., winter (December–February; DJF), spring (March–May; MAM), summer (June–August; JJA), and autumn (September–November; SON)]. The diurnal periods are defined based on the relationship of solar elevation angle to solar noon, with the morning and evening periods corresponding to the ML growth and decay transition periods, respectively (e.g., Seidel et al. 2010). The atmospheric stability conditions are determined from mean Ri_B values below 0.20 km as follows: first, unstable for values less than −0.01; second, near neutral for values between or equal to −0.01 and 0.01; and third, stable for values greater than 0.01. To ensure that the nocturnal cases have sufficient friction velocity to support mechanical mixing conditions, only cases with mean surface wind speeds greater than $2\,\mathrm{m\,s^{-1}}$ are used in the analysis (Goulden et al. 1996) with the surface winds, including those below 0.20 km. Last, sky obscuration conditions are categorized into cloudy, elevated aerosol layer (EAL), and clear-sky conditions. A lidar's signal quality is sensitive to sky obscuration conditions and its backscatter profile can be greatly complicated as a result. Therefore, the dependence of the H_L methods on sky obscurations is of great interest. To determine cloudy conditions, a threshold method is applied to ASR observations to discern from EAL and clear-sky situations (Baars et al. 2008). Baars et al. (2008) used the WCT method with a C' threshold value of −0.1 to identify cloud bases, and this study uses a −0.25 threshold value over a dataset with higher spatial resolution. The EAL conditions are identified by mean ASR above 0.80 km (an empirical height) being greater than mean ASR below with no clouds present. The clear-sky group makes up the remainder of the sky obscuration conditions.

4. Results and analysis

There are 4030 coincident lidar and radiosonde soundings examined for ML height. Figure 2 shows the distribution of the sounding cases by stability in terms of diurnal periods. There are 2427, 1328, and 275 cases of stable, unstable, and near-neutral stability conditions, respectively. Unfortunately, there are only a few morning cases and an abundance of night cases. The skewed ratio of night to morning cases is the result of the timing of the radiosoundings and the defining of night and morning periods. For an example, the after sunrise radiosonding is scheduled for 1200 UTC and the summer morning (ML growth) transitional period is roughly from 1400 UTC (0800 LT) to 1630 UTC (1030 LT). Therefore, this sounding is recognized as a night case. Table 2 provides the distribution of the test cases by atmospheric stability and sky obscuration conditions with the population size parameter (N). The EAL condition occurred the most frequently among the sky obscuration conditions. Its frequent occurrence corresponds to the high occurrence of the night and stable cases in which conditions are conducive for stratified layers.

a. Reference method

The reference ML height measurements H_{RS} were compared to those attained by the profile gradient methods (θ_v, q, or M). This comparison examined the consensus of H_{RS} and the closest profile gradient method that compared within ±0.25 km. Overall, H_{RS} exhibited an RMSE of ±0.09 km with a coefficient of determination of 0.93 and a linear regression slope of 0.98. Its greatest consensus was found for stable conditions

TABLE 2. Consistency rates (Co), mean bias (μ), and RMSE of $H_L - H_{RS}$ categorized by atmospheric stability and sky obscuration conditions. The Co parameter provides the percentage of differences that are less than ±0.30 km. The mean bias and RMSE values are measured in kilometers.

		Hybrid (%), (km)			Hybrid-lowest (%), (km)			WCT (%), (km)			ERF (%), (km)		
	N	Co	μ	RMSE	Co	μ	RMSE	Co	μ	RMSE	Co	μ	RMSE
All	4030	60	0.24	0.52	61	−0.22	0.51	65	0.15	0.48	50	0.19	0.63
Stable	2427	54	0.28	0.53	74	−0.09	0.34	67	0.12	0.43	55	0.23	0.52
Unstable	1328	71	0.15	0.48	42	−0.44	0.71	65	0.18	0.53	42	0.14	0.79
Neutral	275	57	0.28	0.58	36	−0.29	0.53	50	0.21	0.57	48	0.13	0.62
EAL	2075	55	0.30	0.58	58	−0.23	0.54	62	0.18	0.52	46	0.24	0.69
Cloudy	1145	66	0.04	0.43	55	−0.28	0.54	65	0.08	0.46	59	0.05	0.52
Clear	810	65	0.21	0.44	75	−0.09	0.38	73	0.11	0.38	50	0.28	0.62

(±0.09 km) and least for near-neutral conditions (±0.12 km). These results add confidence regarding the reliability of H_{RS}. In addition, Fig. 3 displays seasonal trihourly averaged H_{RS} measurements. It captures wintertime's seasonal low and summertime's seasonal high for midday ML heights over SGP.

b. Lidar detection methods

The comparison results of the H_L methods and H_{RS} observations are tabulated in Table 2 by atmospheric stability and sky obscuration conditions. Table 2 provides their mean biases, RMSE, and consistency rates. The consistency rate parameter indicates the percentage of the H_L observations that measured within ±0.30 km of H_{RS}.

The overall statistical results of Table 2 show that the performance of the new method approaches is similar with averaged absolute biases of about 0.23 ± 0.52 km and consistency rates slightly greater than 60%. In addition, the new method approaches are more efficient overall than the modified ERF method but less than the WCT method. However, they do show individual efficiencies in certain meteorological conditions over the WCT method. Table 2 shows the hybrid method having skill advantages in the unstable and cloudy categories, with consistency rates of 71% and 66% and mean errors of 0.15 ± 0.48 and 0.14 ± 0.43 km, respectively. The unstable ML is characterized by thermally driven turbulence and a top that normally corresponds to the peak gradient of a backscatter profile (Hennemuth and Lammert 2006). This also represents the condition of a cloudy/unstable ML, which occurred in 37% of the cloudy cases. The success of the hybrid method in these two categories stems from its dependence on peak gradients and the effectiveness of the LCL height constraint method to restrict its detection range below decoupled clouds for the more stable/cloudy situations. In addition, Table 2 shows the hybrid-lowest method having skill advantages in the stable and clear-sky categories, with consistency rates of 74% and 75% and mean errors

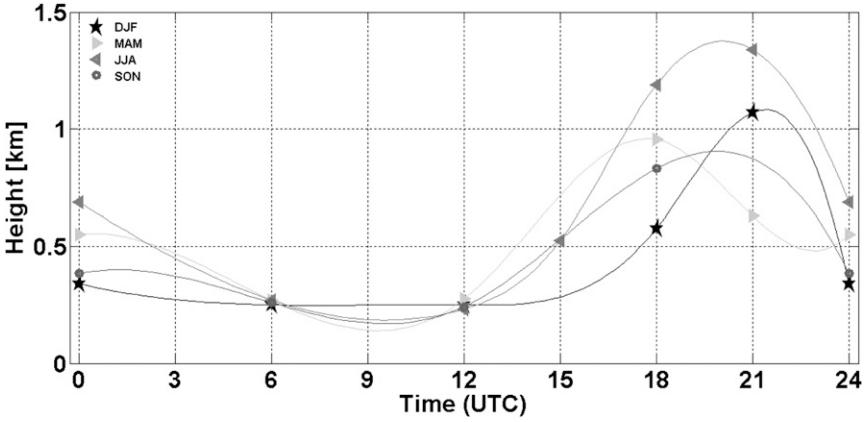

FIG. 3. Averaged trihourly diurnal ML heights taken from radiosonde observations (H_{RS}) per meteorological season: winter (DJF), spring (MAM), summer (JJA), and autumn (SON). The abscissa is time (UTC), and the ordinate is height (km). Routine radiosounding observation hours are 0000, 6000, 1200, and 1800 UTC. The mixing height averages at 2100 UTC are from special soundings.

of −0.09 ± 0.34 and −0.09 ± 0.38 km, respectively. The stable ML consists of suppressed mixing conditions and a top that can blend into the residual layer, leaving a weak gradient associated with it. The effectiveness of the hybrid-lowest method relates to its partial independence on the peak gradient and its ability to inspect below elevated obscurations for ML height. In clear-sky conditions, the ML is apt to behave more ideally, which explains the relatively good performance of almost all the H_L methods. The high occurrence of stable conditions in this category explains why the hybrid-lowest method performed the best of the methods, with 70% of the cases being stable. Moreover, Table 2 shows the H_L methods having the least success with EAL and near-neutral conditions, with average consistency rates of 55% and 48% and mean errors of 0.12 ± 0.58 and 0.08 ± 0.58 km, respectively. The EAL condition can consist of thermally stratified layers above the ML height, which can produce spurious gradients that complicate the layer attribution process (e.g., Hennemuth and Lammert 2006). Contrarily, the near-neutral condition can consist of a lack of thermal stratification and a poorly defined ML height, which produces a complex aerosol structure that also complicates the layer attribution process. The WCT and hybrid methods performed the best for EAL and near-neutral conditions, with 62% and 57% consistency rates, respectively. More research is needed to improve the performance of H_L methods in both conditions, along with an evaluation of the suitability of using aerosols as proxies, especially for near-neutral conditions.

To qualitatively evaluate the effectiveness of the H_L methods, the results of this study were compared to those of similar studies that used H_{RS} as an independent reference. Haeffelin et al. (2012) used the consistency rate parameter, also with a threshold of ±0.30 km, for nighttime and daytime conditions to evaluate the structure of the atmosphere (STRAT-2D) detection algorithm and others. For nighttime conditions, Haeffelin et al. achieved consistency rates as high as 33% and for daytime conditions as high as 67%. In contrast, this study achieved consistency rates of 75%, 60%, 73%, and 60% for the hybrid-lowest, hybrid, WCT, and ERF methods in nighttime conditions, respectively. For daytime conditions, consistency rates attained were 45%, 72%, 64%, and 43%, respectively. Relative to Haeffelin et al., the H_L methods of this study offered higher consistency rates for nighttime conditions, which is a direct result of the application of the LCL height constraint, and for daytime conditions, the hybrid and WCT methods produced consistency rates of equivalence. Luo et al. (2014) also used the consistency rate parameter but determined it by percentage differences. They evaluated the gradient detection method under cloud-free daytime conditions for the same geographical location (SGP) and within the same test period (2007–09) with a micropulse lidar system. They used a threshold of 30% and achieved a consistency rate of 74%. In contrast, using percentage differences over all daytime conditions, this study achieved consistency rates ranging from 38% to 70%. The hybrid and hybrid-lowest methods made up the upper and lower ends of this range, respectively. Studies have also evaluated H_L methods by examining biases for daytime conditions (Granados-Muñoz et al. 2012; Milroy et al. 2012; Yang et al. 2013; Luo et al. 2014); results ranged from 0.04 ± 0.27 km (Luo et al. 2014) to 0.15 ± 0.18 km (Milroy et al. 2012). This study attained an averaged bias of 0.19 ± 0.50 km for the more efficient daytime methods (WCT and hybrid). The daytime bias of the hybrid and WCT methods are in fairly good agreement with the previous studies. The other two methods (ERF and hybrid-lowest) are not, possibly due to their oversensitivity to spurious gradients and structures in backscatter profiles; in particular, the hybrid-lowest method suffers from misinterpreting valley gradients as elevated obscurations in daytime MLs. These elevated obscurations can sometime reside in the daytime ML or be coupled to the daytime ML top. The ERF and hybrid-lowest method average daytime H_L bias is −0.06 ± 0.71 km. The above-mentioned qualitative comparison results provide context to the reliability of the new and component methods, which appear to be as reliable as the H_L methods they are compared against. The relatively good comparison results to the prior studies, which were mostly evaluated under less complex conditions, are credited to the effectiveness of the LCL height constraint.

c. *Case studies*

Figure 4 displays case studies of the H_L methods for stable, unstable and near-neutral ML conditions. These cases illustrate some of the strengths and weaknesses of the H_L methods. The corresponding ASR and ancillary (θ_v, M, and q) profiles and the H_{RS} measurements are provided for each case.

Figure 4a presents a stable ML case with a clear-sky and well-defined residual layer occurring at 2340 UTC 10 March 2007. It demonstrates the difficulty of conducting layer attribution with aerosol backscatter observations for a stable ML. Without a priori knowledge of the ML being stable, the gradient peak of the residual layer top can easily be mistaken as ML height. The H_{RS} method selects ML height at 0.20 km. The top of the θ_v inversion and M profile's gradient maxima support this approximation. The q profile exhibits a very tenuous kink around the H_{RS} estimate but is too weak to interpret as support for the H_{RS} estimate. Nevertheless,

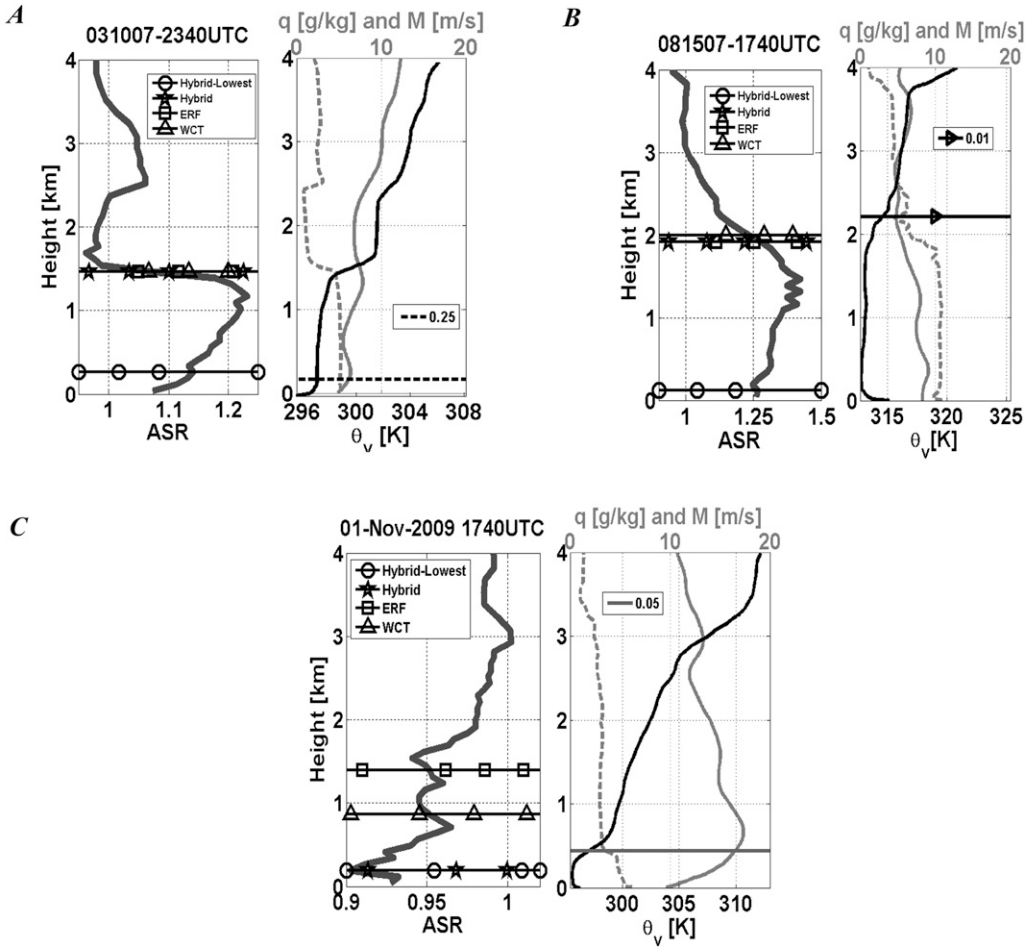

FIG. 4. Case studies for detecting mixing heights during (a) stable, (b) unstable, and (c) near-neutral stability conditions. Each panel consist of (left) an ASR profile with lidar-based mixing height estimates horizontally overlaid and (right) radiosoundings of potential temperature (black), wind speed (gray), and specific humidity (gray dashed line) with an independent reference mixing height estimate horizontally overlaid. Critical bulk Richardson numbers 0.25, 0.01, and 0.05 are used for the stable, unstable, and near-neutral stability cases, respectively.

the H_{RS} estimate is accepted as reliable based on its agreement with the θ_v and M gradient methods. Of the H_L methods, the hybrid-lowest method determines H_L below the residual layer near H_{RS}. It accomplishes this due to the valley gradient at 0.42 km with the $3\Delta C'$ profile. The LCL height constraint restricts the ML height detection range of this backscatter profile below 2.22 km. The other methods incorrectly select the residual layer top, at 1.47 km, as ML height due to the strong gradient there. The gradient maxima selected by the hybrid-lowest method in the ASR profile as ML height is a product of the more dispersible aerosol condition of the decoupled residual layer relative to the ML. The relative smooth curve of the backscatter profile in the ML to that of the adjacent residual layer demonstrates this point. This case shows the efficiency of the hybrid-lowest method for stable conditions.

Figure 4b presents a daytime unstable ML case with an entrained EAL at 1740 UTC 15 August 2007. The EAL can be observed between 1 and 2 km with a razor-edge appearance. The result of this case for the H_L methods is opposite of Fig. 4a. The H_{RS} method detects ML height at 2.20 km. Its estimate is supported by all of the ancillary gradient methods with a slight indication of it overestimating ML height by approximately 0.20 km. The hybrid-lowest method greatly underestimates ML height due to the gradient valley generated by the entrained EAL at 1.09 km, while the other H_L methods correctly select the peak gradient at 1.95 km as ML height. This is a relatively simple case with the top of the ML resembling the transition layer of an ideal backscatter profile. It displays the independence of the hybrid-lowest method on the peak gradient when elevated obscurations are present in daytime MLs, which

can be problematic when such obstacles reside within the ML. In addition, this case displays the importance of the quality control process for H_{RS} measurements. It ensures the reliability of the H_{RS} method within ± 0.25 km.

Last, Fig. 4c displays a daytime near-neutral ML case with low aerosol loading and strong winds occurring at 1740 UTC 1 November 2009. For this case, H_{RS} locates the ML height at 0.43 km. The θ_v and q profiles support this estimate and the M profile places the ML height slightly higher by about 0.25 km. The new method approaches underestimate H_{RS}, while the two component methods overestimate it. The windy and near-neutral conditions allow aerosols to efficiently ventilate and disperse, which explain the variability of the H_L estimates. The tenuous kink in the ASR profile around 0.40 km seems to correspond to the H_{RS} observation, but its gradient strength is overshadowed by those above and below it. This is a case of the thermodynamic and aerosol profiles being inconsistent, which is a common occurrence in near-neutral conditions (e.g., Emeis et al. 2008; Pearson et al. 2010). This type of occurrence makes the layer attribution process very difficult to automate. Further research on determining H_L for near-neutral MLs is warranted, along with how dependable aerosols are as proxies.

5. Summary and discussion

A new method for automatically attaining ML heights with lidar backscatter data was presented and evaluated in a variety of meteorological conditions. It was applied in two ways: 1) by looking for the most realistic ML height throughout the entire profile and 2) by searching for ML height below significant elevated obscurations (e.g., clouds and aerosol layers). These two approaches were called the hybrid and hybrid-lowest methods, respectively. Their robustness was compared to their component methods (WCT and modified ERF), and the meteorological conditions in which the respective methods performed the most optimally were identified (see Table 2). In addition, a new surface-based ML height constraint technique and an approach for evaluating H_L methods by sky obscuration conditions were presented.

The new method approaches offered some advantages over the component methods. The hybrid method exhibited advantages in unstable and cloudy conditions. In general, it proved to be more reliable than the ERF method and comparative to the WCT method in those conditions. The hybrid-lowest method offered skill improvements in stable and clear-sky meteorological conditions. It was significantly more efficient in stable conditions than all other methods. The WCT method proved to be the most reliable method overall.

The overall performance of the H_L methods was compared to other studies that used H_{RS} measurements as independent references but, generally, over shorter study periods and during less complex meteorological conditions. Nevertheless, the results of this study proved to be equivalent for unstable conditions and improved for stable conditions. This outcome is largely due to the application of the LCL height constraint. Its application improved the results by an average of 0.27 km per meteorological condition.

This study shows a potential to achieve close to a 70% consistency rate or higher for every meteorological condition, except elevated aerosol layers (EAL) and near-neutral conditions, if the H_L methods are optimally used in their preferred conditions. This supports Haeffelin et al.'s (2012) postulation that knowing the stability of the atmosphere can improve layer attribution, and it also shows the value of knowing sky obscuration conditions. For example, knowing that the sky is obscured by an EAL and that the ML is stable may prompt an algorithm to be skeptical of a gradient peak and use a method more like the hybrid-lowest method to determine H_L. The more metadata that can be gathered prior to performing layer attribution, the more confidence an H_L algorithm can have in its selection. More research is required for near-neutral and EAL conditions to increase the robustness of H_L methods and to better understand the viability of using aerosols as proxies. Also, similar analysis in other climate regimes is recommended to confirm the tendencies of the H_L methods.

Acknowledgments. This research was partially funded by the NOAA Educational Partnership Program Grant NA17AE1625 and NOAA Grant NA17AE1623 to establish the NOAA Center for Atmospheric Sciences (NCAS) at Howard University. It was also partially funded by the National Atmospheric and Space Administration (NASA) Research Cooperative Agreement NNX08BA42A. The authors acknowledge the U.S. Department of Energy, Office of Science, ARM Climate Research Facility for making such a rich dataset of atmospheric observations readily available. The authors also acknowledge the anonymous reviewers and journal editor who provided helpful insight and valuable comments.

REFERENCES

Angelini, F., F. Barnaba, T. C. Landi, L. Caporaso, and G. P. Gobbi, 2009: Study of atmospheric aerosols and mixing layer by LIDAR. *Radiat. Prot. Dosim.*, **137**, 275–279, doi:10.1093/rpd/ncp219.

ARM, 1994: Balloon-borne sounding system (SONDEWNPN), Southern Great Plains (SGP) Central Facility. ARM Climate Research Facility Data Archive, subset used: January

2006–December 2010, accessed 11 February 2011, doi:10.5439/1021460.

——, 2004: Raman lidar vertical profiles (10RLPROFBE1NEWS), Southern Great Plains (SGP) Central Facility. ARM Climate Research Facility Data Archive, subset used: January 2006–December 2010, accessed 11 February 2011, doi:10.5439/1027250.

Baars, H., A. Ansmann, R. Engelmann, and D. Althausen, 2008: Continuous monitoring of the boundary-layer top with lidar. *Atmos. Chem. Phys.*, **8**, 7281–7296, doi:10.5194/acp-8-7281-2008.

Baxter, R. A., 1991: Determination of mixing heights from data collected during the 1985 SCCCAMP field program. *J. Appl. Meteor.*, **30**, 598–606, doi:10.1175/1520-0450(1991)030<0598:DOMHFD>2.0.CO;2.

Beyrich, F., 1997: Mixing height estimation from sodar data—A critical discussion. *Atmos. Environ.*, **31**, 3941–3952, doi:10.1016/S1352-2310(97)00231-8.

Boers, R., E. W. Eloranta, and R. L. Coulter, 1984: Lidar observations of mixed layer dynamics: Tests of parameterized entrainment models of mixed layer growth rate. *J. Climate Appl. Meteor.*, **23**, 247–266, doi:10.1175/1520-0450(1984)023<0247:LOOMLD>2.0.CO;2.

Davis, K. J., D. H. Lenschow, S. P. Oncley, C. Kiemle, G. Ehret, A. Giez, and J. Mann, 1997: Role of entrainment in surface-atmosphere interaction over the boreal forest. *J. Geophys. Res.*, **102**, 29 219–29 230, doi:10.1029/97JD02236.

——, N. Gamage, C. R. Hagelberg, C. Kiemle, D. H. Lenschow, and P. P. Sullivan, 2000: An objective method for deriving atmospheric structure from airborne lidar observations. *J. Atmos. Oceanic Technol.*, **17**, 1455–1468, doi:10.1175/1520-0426(2000)017<1455:AOMFDA>2.0.CO;2.

Emeis, S., K. Schäfer, and C. Münkel, 2008: Surface-based remote sensing of the mixing-layer height—A review. *Meteor. Z.*, **17**, 621–630, doi:10.1127/0941-2948/2008/0312.

Ferrare, R. A., and Coauthors, 2006: Evaluation of daytime measurements of aerosols and water vapor made by an operational Raman over the Southern Great Plains. *J. Geophys. Res.*, **111**, D05S08, doi:10.1029/2005JD005836.

Flamant, C., J. Pelon, P. H. Flamant, and P. Durand, 1997: Lidar determination of the entrainment zone thickness at the top of the unstable air in atmospheric boundary layer. *Bound.-Layer Meteor.*, **83**, 247–284, doi:10.1023/A:1000258318944.

Goldsmith, J. E. M., F. H. Blair, S. E. Bisson, and D. D. Turner, 1998: Turn-key Raman lidar for profiling atmospheric water vapor, clouds, and aerosols. *Appl. Opt.*, **37**, 4979–4990, doi:10.1364/AO.37.004979.

Goulden, M. L., J. W. Munger, S.-M. Fan, B. C. Daube, and S. C. Wofsy, 1996: Measurements of carbon sequestration by long-term eddy covariance: methods and a critical evaluation of accuracy. *Global Change Biol.*, **2**, 169–182, doi:10.1111/j.1365-2486.1996.tb00070.x.

Granados-Muñoz, M. J., F. Navas-Guzmán, J. A. Bravo-Aranda, J. L. Guerrero-Rascado, H. Lyamani, J. Fernández-Gálvez, and L. Alados-Arboledas, 2012: Automatic determination of the planetary boundary layer height using lidar: One-year analysis over southeastern Spain. *J. Geophys. Res.*, **117**, D18208, doi:10.1029/2012JD017524.

Haeffelin, M., and Coauthors, 2012: Evaluation of mixing-height retrievals from automated profiling lidars and ceilometers in view of future integrated networks in Europe. *Bound.-Layer Meteor.*, **143**, 49–75, doi:10.1007/s10546-011-9643-z.

Hageli, P., D. G. Steyn, and K. B. Strawbridge, 2000: Spatial and temporal variability of mixed-layer depth and entrainment zone thickness. *Bound.-Layer Meteor.*, **97**, 47–71, doi:10.1023/A:1002790424133.

Hennemuth, B., and A. Lammert, 2006: Determination of the atmospheric boundary layer height from radiosonde and lidar backscatter. *Bound.-Layer Meteor.*, **120**, 181–200, doi:10.1007/s10546-005-9035-3.

Jeričević, A., and G. Grisogono, 2006: The critical bulk Richardson number in urban areas: Verification and application in a numerical weather prediction model. *Tellus*, **58A**, 19–27, doi:10.1111/j.1600-0870.2006.00153.x.

Lawrence, M., 2005: The relationship between relative humidity and the dewpoint temperature in moist air: A simple conversion and applications. *Bull. Amer. Meteor. Soc.*, **86**, 225–233, doi:10.1175/BAMS-86-2-225.

Liu, S., and X. Liang, 2010: Observed diurnal cycle climatology of planetary boundary layer height. *J. Climate*, **23**, 5790–5809, doi:10.1175/2010JCLI3552.1.

Luo, T., R. Yuan, and Z. Wang, 2014: Lidar-based remote sensing of atmospheric boundary height over land and ocean. *Atmos. Meas. Tech.*, **7**, 173–182, doi:10.5194/amt-7-173-2014.

Martucci, G., R. Matthey, and V. Mitev, 2007: Comparison between backscatter lidar and radiosonde measurements of the diurnal and nocturnal stratification in the lower troposphere. *J. Atmos. Oceanic Technol.*, **24**, 1231–1244, doi:10.1175/JTECH2036.1.

Melfi, S. H., J. D. Spinhirne, S. H. Chou, and S. P. Palm, 1985: Lidar observations of vertically organized convection in the planetary boundary layer over the ocean. *J. Climate Appl. Meteor.*, **24**, 806–821, doi:10.1175/1520-0450(1985)024<0806:LOOVOC>2.0.CO;2.

Menut, L., C. Flamant, J. Pelon, and P. H. Falmant, 1999: Urban boundary-layer height determination from lidar measurements over Paris area. *Appl. Opt.*, **38**, 945–954, doi:10.1364/AO.38.000945.

Milroy, C., and Coauthors, 2012: An assessment of pseudo-operational ground-based light detection and ranging sensors to determine the boundary-layer structure in the coastal atmosphere. *Adv. Meteor.*, **2012**, 929080, doi:10.1155/2012/929080.

Pearson, G., F. Davies, and C. Collier, 2010: Remote sensing of the tropical rain forest boundary layer using pulsed Doppler lidar. *Atmos. Chem. Phys.*, **10**, 5891–5901, doi:10.5194/acp-10-5891-2010.

Piironen, A. K., and E. W. Eloranta, 1995: Convective boundary layer depths and cloud geometerical properties obtained from volume imaging lidar data. *J. Geophys. Res.*, **100**, 25 569–25 576, doi:10.1029/94JD02604.

Revercomb, H. E., and Coauthors, 2003: The ARM Program's water vapor intensive observation periods—Overview, initial accomplishments, and future challenges. *Bull. Amer. Meteor. Soc.*, **84**, 217–236, doi:10.1175/BAMS-84-2-217.

Schmid, P., and D. Niyogi, 2012: A method for estimating planetary boundary layer heights and its application over the ARM Southern Great Plains site. *J. Atmos. Oceanic Technol.*, **29**, 316–322, doi:10.1175/JTECH-D-11-00118.1.

Seibert, P., F. Beyrich, S. E. Gryning, S. Joffre, A. Rassumussen, and P. Tercier, 2000: Review and intercomparison of operational methods for the determination of the mixing height. *Atmos. Environ.*, **34**, 1001–1027, doi:10.1016/S1352-2310(99)00349-0.

Seidel, D. J., C. O. Ao, and K. Li, 2010: Estimating climatological planetary boundary layer heights from radiosonde observations: Comparison of methods and uncertainty analysis. *J. Geophys. Res.*, **115**, D16113, doi:10.1029/2009JD013680.

——, Y. Zhang, A. Beljaars, J.-C. Golaz, A. R. Jacobson, and B. Medeiros, 2012: Climatology of the planetary boundary layer over the continental United States and Europe. *J. Geophys. Res.*, **117**, D17106, doi:10.1029/2012JD018143.

Senff, C., J. Bösenberg, G. Peters, and T. Schaberl, 1996: Remote sensing of turbulent ozone fluxes and the ozone budget in the convective boundary layer with DIAL and radar-RASS: A case study. *Contrib. Atmos. Phys.*, **69**, 161–176.

Steyn, D. G., M. Baldi, and R. Hoff, 1999: The detection of mixed layer depth from lidar backscatter profiles. *J. Amos. Oceanic Technol.*, **16**, 953–959, doi:10.1175/1520-0426(1999)016<0953:TDOMLD>2.0.CO;2.

Stokes, G. M., and S. E. Schwartz, 1994: The Atmospheric Radiation Measurement (ARM) Program: Programmatic background and design of the Cloud and Radiation Test Bed. *Bull. Amer. Meteor. Soc.*, **75**, 1201–1221, doi:10.1175/1520-0477(1994)075<1201:TARMPP>2.0.CO;2.

Turner, D. D., R. A. Ferrare, L. A. Heilman Brasseur, W. F. Feltz, and T. P. Tooman, 2002: Automated retrievals of water vapor and aerosol profiles from an operational Raman lidar. *J. Atmos. Oceanic Technol.*, **19**, 37–50, doi:10.1175/1520-0426(2002)019<0037:AROWVA>2.0.CO;2.

Yang, D., C. Li, A. K. Lau, and Y. Li, 2013: Long-term measurement of daytime atmospheric mixing layer height over Hong Kong. *J. Geophys. Res. Atmos.*, **118**, 2422–2433, doi:10.1002/jgrd.50251.

Zilitinkevich, S. S., and A. Baklanov, 2002: Calculation of the height of stable boundary layers in practical applications. *Bound.-Layer Meteor.*, **105**, 389–409, doi:10.1023/A:1020376832738.